

## Supplementary Material

Jun Ruan, Yixuan Li, Junzhe Lin, Zihan Ren, Naeem Iqbal, Dan Guo\*, Tianrui Zhai \*

# **Transferable microfiber laser arrays for high-sensitivity thermal sensing**

*College of Physics and Optoelectronics, Faculty of Science, Beijing University of Technology, Beijing 100124, China.*

\*E-mail: trzhai@bjut.edu.cn; dguo@bjut.edu.cn

## Contents

<b>1. Supplementary Notes .....</b>	<b>2</b>
<b>2. Supplementary Figures and Table .....</b>	<b>3</b>

# 1. Supplementary Notes

For WGM laser devices, resonant wavelength is determined by cavity radius, microcavity refractive index, ambient refractive index, radial mode number and angular mode number. It can be expressed by following equation:<sup>1</sup>

$$\lambda^{-1}(D, n_{cav}, n_r, r, m) = \frac{1}{\pi n_{cav} D} \left[ m + \frac{1}{2} + 2^{-\frac{1}{3}} \alpha(r) \left( m + \frac{1}{2} \right)^{\frac{1}{3}} - \frac{L}{(n_r^2 - 1)^{\frac{1}{2}}} + \frac{3}{10} 2^{-\frac{2}{3}} \alpha^2(r) \left( m + \frac{1}{2} \right)^{-\frac{1}{3}} - 2^{-\frac{1}{3}} L (n_r^2 - \frac{2}{3} L^2) \frac{\alpha(r) (m + \frac{1}{2})^{-\frac{1}{3}}}{(n_r^2 - 1)^{\frac{3}{2}}} \right] \quad (1)$$

Where  $\lambda$  is the resonant wavelength,  $D$  is cavity diameter,  $n_{cav}$  is the cavity refractive index,  $r$  is radial mode number,  $m$  is angular mode number,  $n_{env}$  is ambient refractive index,  $n_r = n_{cav}/n_{env}$ ,  $\alpha$  is the roots of the Airy function, which equals 2.338 if  $r = 1$ ,  $L = 1/n_r$ , for TM modes and  $L = n_r$ , for TE modes.

According to the above equation, it can be seen that the resonant wavelength will blue shift when the cavity refractive index  $n_{cav}$  and ambient refractive index  $n_{env}$  decrease. As the thermo-optic coefficient of PVA and PDMS is negative and its thermo-expansion coefficient is positive, as well as the thermo-expansion coefficient is negligible, the refractive index of PVA and PDMS will decrease with increasing temperature. Thus, the lasing spectrum of the optoplasmonic hybrid system should exhibit blueshift when the ambient temperature increase, which is consistent with the experimental result.

PDMS acts as the ambient medium when the microfiber is covered by it. The ambient refractive index (RI) of the microresonator is variable with the temperature owing to high TO coefficient of PDMS. The RI of the PDMS is about 1.4176. As the TO coefficient of PDMS is  $-4.5 \times 10^{-4}$ , the RI of PDMS ( $n_{PDMS}$ ) as the function of temperature ( $T$ ) can be expressed as follows:<sup>2</sup>

$$n_{PDMS} = -4.5 \times 10^{-4} \cdot T + 1.4176 \quad (1)$$

When the temperature rises from 30.6 °C to 38.7 °C,  $n_{PDMS}$  decreases from 1.4038 to 1.4002. The contribution of PDMS to the wavelength shift of a specific WGM lasing microfiber when temperature changes can be calculated by equation (1). The RI of the microfiber is measured to be 1.58. Assume the diameter of the pristine dye-doped PVA microfiber is 40  $\mu\text{m}$ , we substitute the variation of  $n_{PDMS}$  in equation (1), it can be calculated that the resonance wavelength exhibits a blueshift from 627.797 nm to 627.846 nm for the angular mode number of 305 (Fig. S12). Thus, the corresponding contribution of PDMS to thermal sensing sensitivity is 0.006 nm/°C.

## 2. Supplementary Figures

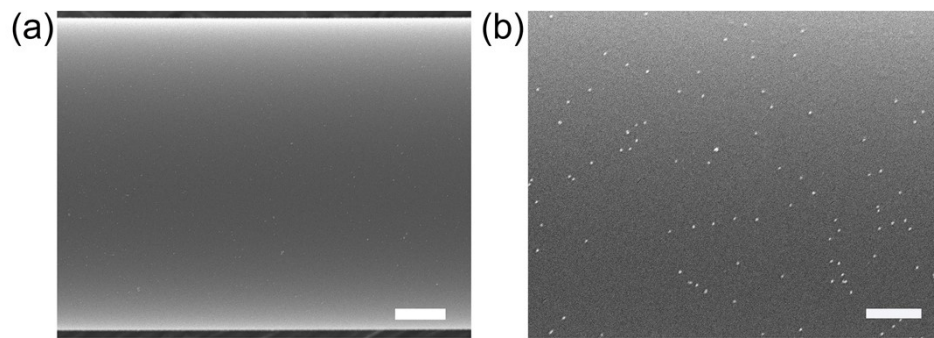


**Fig. S1** (a) SEM image of the Au NRs-decorated microfiber. Scale bar: 5  $\mu\text{m}$ . (b) High magnification from Fig. S1(a). Scale bar: 2  $\mu\text{m}$ .

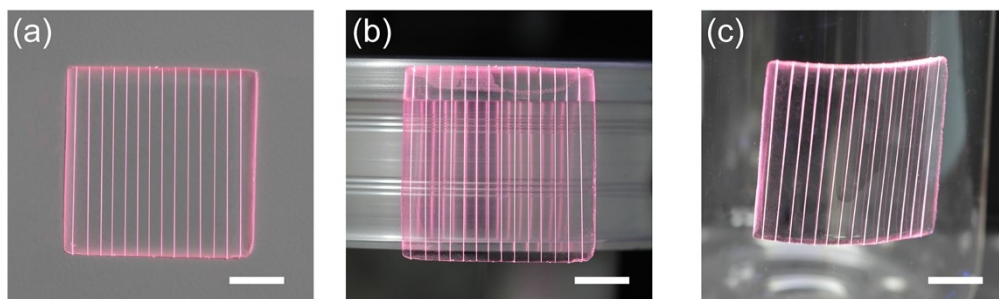


**Fig. S2** The transferable membrane attached to the laboratory wall (a), the uneven rounded corners at the edge of the table (b), and the outer wall of glass beaker (c). Scale bar: 1 cm.

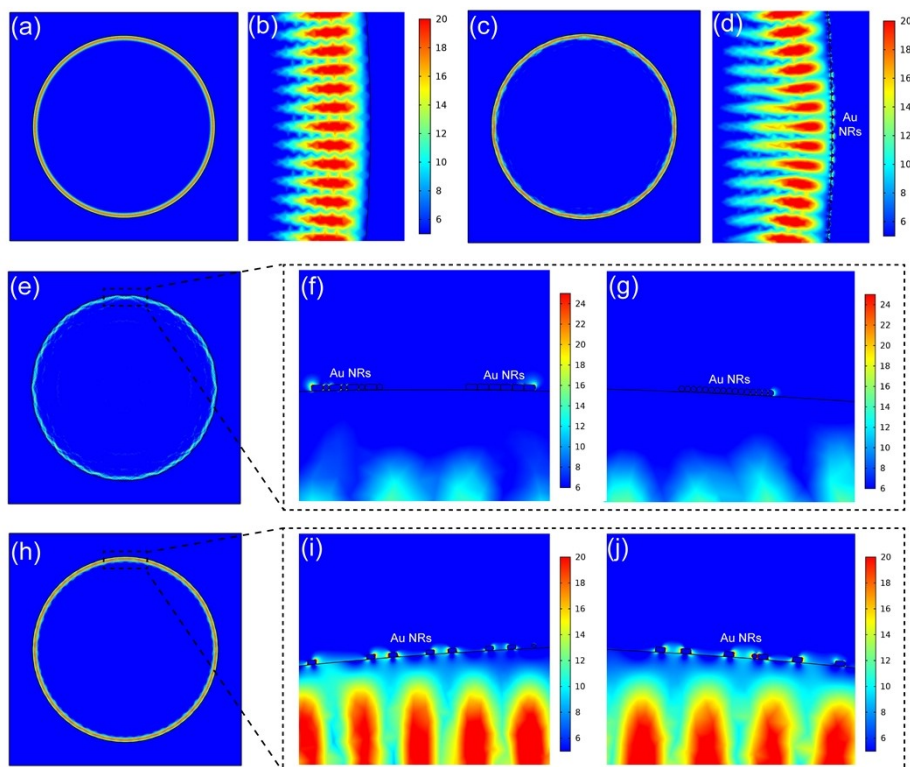


**Fig. S3** Simulated mode field intensity distribution for the microfiber with and without Au NRs attachment for different models in the horizontal plane. (a) Mode field intensity distribution for the pristine microfiber. (b) High magnification from Fig. S2(a). (c) Mode field intensity distribution for the microfiber with periodic Au NRs attachment. (d) High magnification from Fig. S2(c). (e) Mode field intensity distribution for the microfiber with random continuous attachment of Au NRs. (f, g) High magnification from Fig. S3(e). (h) Mode field intensity distribution for the microfiber with random discrete attachment of Au NRs. (i, j) High magnifications from Fig. S3(h).

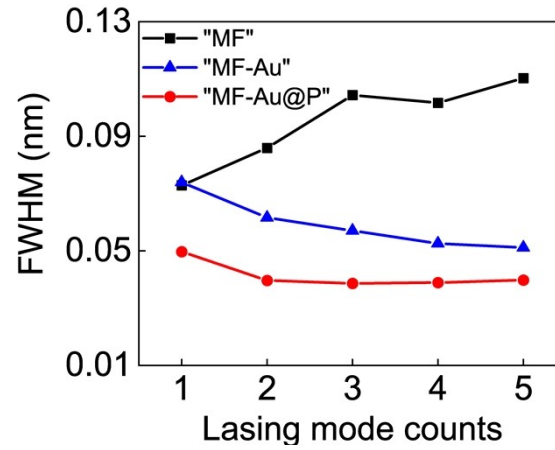


**Fig. S4** The FWHM recorded from lasing modes of the spectra in Figure 2d.

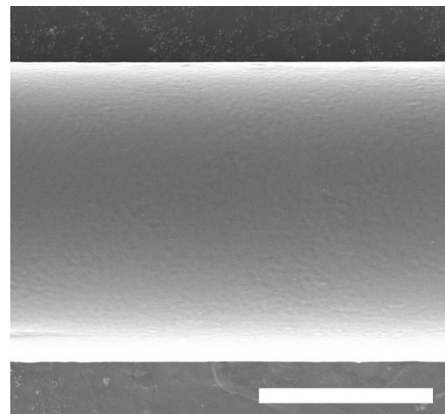


**Fig. S5** SEM image of microfiber with slight roughness surface. Scale bar: 20  $\mu\text{m}$ .

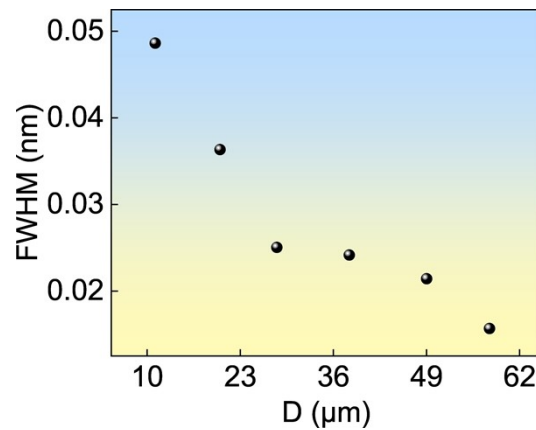


**Fig. S6** The FWHM decreases with diameters of the optoplasmon hybrid microfiber.

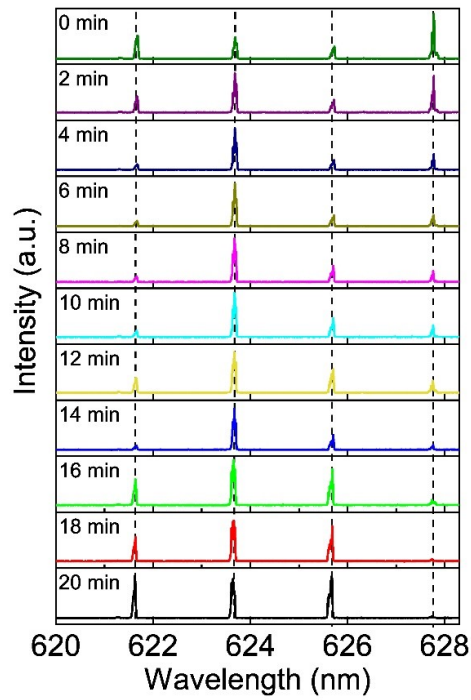


**Fig. S7** Lasing spectra acquired from the temperature sensor of transferable membrane inlaid with WGM-plasmon hybrid microlaser arrays under continuous pumping for 20 minutes.

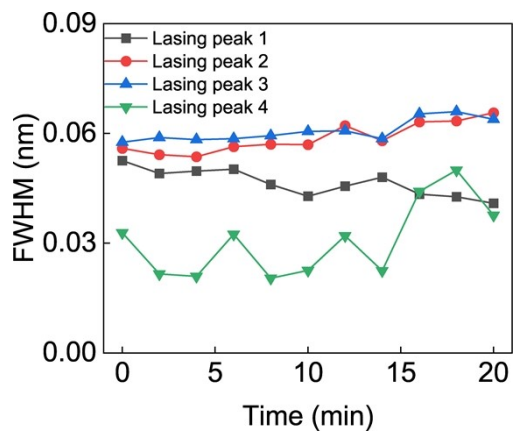


**Fig. S8** The FWHM of the lasing modes under continuous pumping for 20 minutes, showing the stable of this strategy.

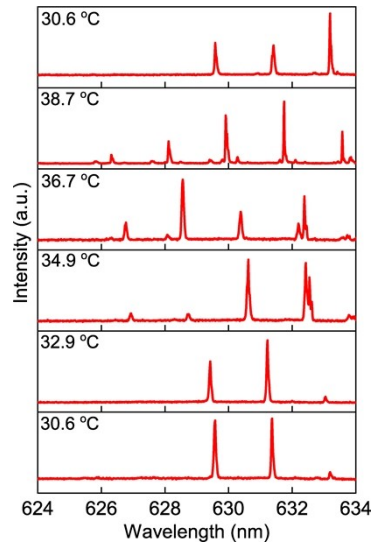


**Fig. S9** Lasing spectra of the transferable membrane inlaid with WGM-plasmon hybrid microlaser arrays under different temperature variations.

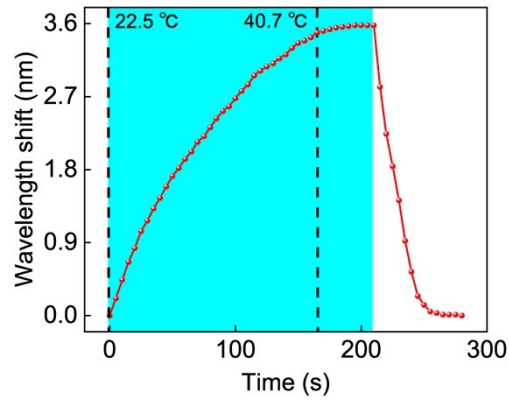


**Fig. S10** Time-dependent shift of the spectral lasing peak position upon heating process.

To demonstrate the thermal sensing performance of the membrane, the dependence of WGM laser wavelength shift on heating time is investigated. Firstly, wavelength blueshift of the lasing peak was observed as soon as the sample was heated. Then, the peak gradually blueshift and tends to saturation when the temperature rises to 40.7 °C. After that, the wavelength slowly moves and gradually reaches equilibrium. Finally, the peak returns to the initial position when the temperature drops to the initial value. The result shows that the optoplasmon in hybrid systems have good responsiveness to temperature changes and show the potential applied in wearable sensing system.

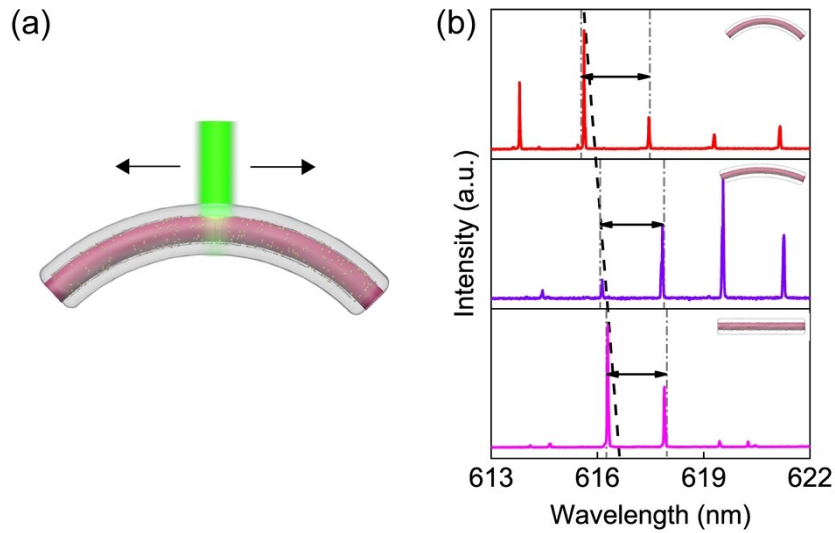


**Fig. S11** (a) Schematic diagram shows the bending of the Au NRs-decorated microfibers inside PDMS elastomer. (b) The lasing emission of “MF-Au@P” structure under different degrees of bending. During the bending, the lasing spectrum exhibits a clear blueshift of 0.665 nm, and FSR gradually increases from 1.578 nm to 1.838 nm. The right top insets show the Au NRs-decorated microfibers in PDMS elastomer under different bending condition.

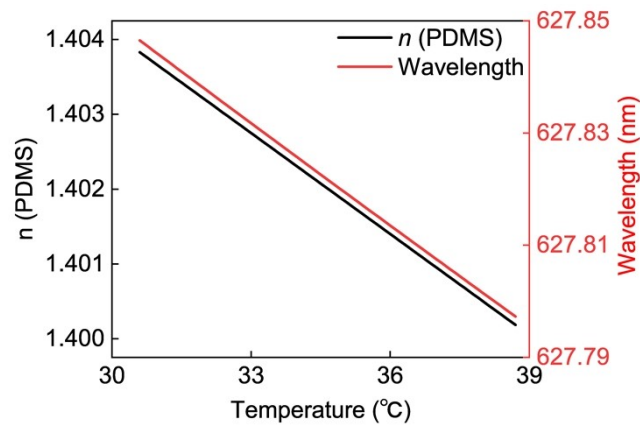


**Fig. S12** The dependence of simulated refractive index of PDMS and wavelength shift on the the temperature variation for “MF-Au@P” structure.

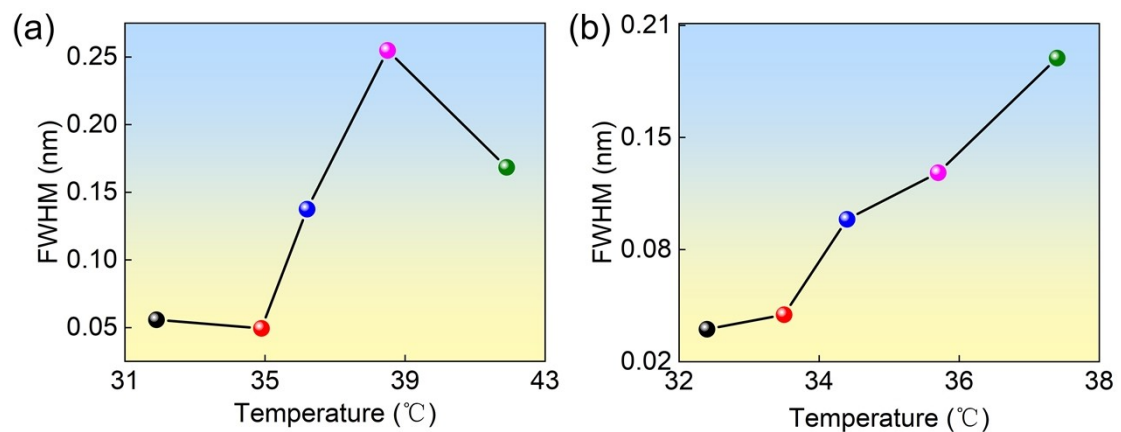


**Fig. S13** The dependence of FWHM of the lasing peak on temperature variation for (a) pristine microfiber and (b)

microfiber in PDMS encapsulation.

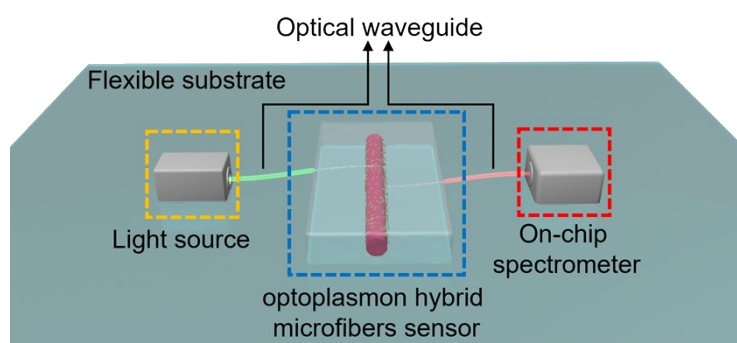


**Fig. S14** Schematic diagram of a transferable optical-based sensing system comprising a light source, an optoplasmon hybrid microfibers sensor, and an on-chip spectrometer.

We attempt to propose a concept of a transferable optical-based sensing system comprising a light source, an optoplasmon hybrid microfibers sensor and an on-chip spectrometer towards the thermal sensing chip. A laser diode can be utilized as a pump source for organic lasing.<sup>3</sup> A micro-spectrometer can be used to analyze the laser sensing signals.<sup>4</sup> The light in and out of the optoplasmon hybrid microfibers sensor can be realized through the on-chip optical waveguides or fibers. In the above way, a portable on-chip integrated thermal sensing system can be realized and applied in real life.

**Table S1** Comparison of thermal sensing performance between different optical-based sensors

Sensor	Material	Temperature sensitivity	Ref.
1	PMMA	-0.011 nm/°C	5
2	PVA	0.079 nm/°C	6
3	PVA	0.153 nm/°C	7
4	UV glue	-0.164 nm/°C	8
5	PVA	-0.181 nm/°C	This work

#### Reference

- 1 S. Yang, Y. Wang and H. Sun, Advances and prospects for whispering gallery mode microcavities, *Adv. Optical Mater.* 2015, **3**, 1136–1162.
- 2 Z. Zhu, L. Liu, Z. Liu, Y. Zhang and Y. Zhang, Surface-plasmon-resonance-based optical-fiber temperature sensor with high sensitivity and high figure of merit, *Opt. Lett.*, 2017, **42**, 2948-2951.
- 3 J. Herrnsdorf, Y. Wang, J. J. D. McKendry, Z. Gong, D. Massoubre, B. Guilhabert, G. Tsiminis, G. A. Turnbull, I. D. W. Samuel, N. Laurand, E. Gu and M. D. Dawson, Micro-LED pumped polymer laser: A discussion of future pump sources for organic lasers, *Laser Photonics Rev.*, 2013, **7**, 1065–1078.
- 4 Z. Yang, T. Albrow-Owen, H. Cui, J. Alexander-Webber, F. Gu, X. Wang, T. C. Wu, M. Zhuge, C. Williams, P. Wang, A. V. Zayats, W. Cai, L. Dai, S. Hofmann, M. Overend, L. Tong, Q. Yang, Z. Sun and T. Hasan, Single-nanowire spectrometers. *Science* 2019, **365**, 1017–1020.
- 5 V. R. Anand, S. Mathew, B. Samuel, P. Radhakrishnan and M. Kailasnath, Thermo-optic tuning of whispering

gallery mode lasing from a dye-doped hollow polymer optical fiber, *Opt. Lett.*, 2017, **42**, 2926-2929.

6 Y.-L. Chou, H.-Y. Wen, Y.-Q. Weng, Y.-C. Liu, C.-W. Wu, H.-C. Hsu and C.-C. Chiang, A U-shaped optical fiber temperature sensor coated with electrospinning polyvinyl alcohol nanofibers: simulation and experiment, *Polymers*, 2022, **14**, 2110.

7 Z. Dong, Y. Jin, G. Zhang, J. Zhou, C. Liu, F. Liu, Z. Wei, F. Wang, C. Tan and H. Meng, Single core-offset Mach-Zehnder interferometer coated with PVA for simultaneous measurement of relative humidity and temperature, *Opt. Express*, 2021, **29**, 24102-24117.

8 S. Wang, Y. Yang, P. Niu, S. Wu, S. Liu, R. Jin, P. Lu, X. Hu and N. Dai, Fiber tip Michelson interferometer for thermal sensing based on polymer-filled suspended core fiber, *Opt. Laser Technol.*, 2021, **141**, 107147.